Nanoscale

PAPER

View Article Online
View Journal | View Issue

Cite this: *Nanoscale*, 2023, **15**, 2904

Photocontrolled DNA nanotubes as stiffness tunable matrices for controlling cellular behavior†

Soumya Sethi,[a] Tomoko Emura,[a] Kumi Hidaka,[a] Hiroshi Sugiyama *[a,b] and Masayuki Endo *[a,b,c]

Received 21st September 2022,
Accepted 16th January 2023

DOI: 10.1039/d2nr05202d

rsc.li/nanoscale

Cell behavior is determined by a variety of properties of the extracellular environment like ligand spacing, nanotopography, and matrix stiffness. Matrix stiffness changes occur during many biological processes like wound healing, tumorigenesis, and development. These spatio-temporal dynamic changes in stiffness can cause significant changes in cell morphology, cell signaling, migration, cytoskeleton *etc*. In this paper, we have created photocontrolled stiffness-tunable DNA nanotubes which can undergo reversible changes in their conformation upon UV and VIS irradiation. When used as a substrate for cell culture, the photocontrolled DNA nanotubes can tune the cell morphology of HeLa cells from a long spindle-shaped morphology with long filopodia protrusions to a round morphology with short filopodia-like extrusions. Such a photocontrolled nanosystem can give us deep insights into the cell–matrix interactions in the native extracellular matrix caused by nanoscopic changes in stiffness.

Introduction

The extracellular matrix (ECM) surrounding the cells undergoes continuous remodeling, especially during the process of development and disease. During tissue development,[1] wound healing,[2] liver fibrosis,[3] glioblastoma,[4] and tumor progression,[5,6] the ECM undergoes various spatial and temporal changes in its stiffness. In the case of tumors, it is seen that the ECM stiffness increases over time and is strongly related to the severity of the disease.[5] The stiffness change of the ECM contributes towards disease progression and there is a need for structurally programmable and dynamic platforms whereby these nanoscale effects of stiffness modulation can be studied on cells in relation to disease development and progression.

Previously researchers have used various polymers and hydrogels to mimic the ECM stiffness changes *in vitro*.[7,8] However, there are no three-dimensional (3D) modular nanoscale level matrices which can dynamically undergo reversible and dynamic stiffness changes to understand various cell–cell and cell–matrix interactions when the matrix is undergoing remodeling. To study such changes on a cellular level, DNA nanotechnology provides an interesting molecular-level toolbox that has excellent programmability for ease of synthesis of cell-guiding biomaterials.[9] Such DNA-based biomaterials have been used in various studies, mostly focusing on the changes in the nanoscale spatial organization of cell adhesion peptides to influence cell morphology.[9–11] It is imperative to note that the dynamic, reversible environment of the ECM is not just limited to the changes in the organization of the cell adhesion peptides. It involves a variety of other changes like stiffness and topology during the process of remodeling.

In this study, using principles of DNA nanotechnology, we have designed photoresponsive 3D DNA nanotubes that can reversibly and dynamically undergo a structural change upon photoirradiation. These DNA nanotubes containing azobenzene photoswitches[12] were designed in a way such that they undergo conformational changes that cause them to change from a fibrous rigid conformation in VIS light to a flexible conformation in UV light (Fig. 1). This 3D fiber-like ECM scaffold was hypothesized to behave as a tunable stiffness matrix for the cells. We observed that these reversible and dynamic stiffness changes are perceived by the cells and they respond to the changes in the matrix by significantly changing their morphology and length of filopodia formed.

Results and discussion

Design of the photocontrolled mechanical DNA nanotubes

We first designed a six-helix bundled DNA nanotube equipped with a conformation-controllable mechanism. As shown in

[a]*Department of Chemistry, Graduate School of Science, Kyoto University, Sakyo-ku, Kyoto 606-8502, Japan. E-mail: endo@kansai-u.ac.jp*
[b]*Institute for Integrated Cell-Material Sciences, Kyoto University, Sakyo-ku, Kyoto 606-8501, Japan*
[c]*Organization for Research and Development of Innovative Science and Technology, Kansai University, Suita, Osaka 564-8680, Japan*

† Electronic supplementary information (ESI) available: Experimental procedures and DNA sequences. See DOI: https://doi.org/10.1039/d2nr05202d

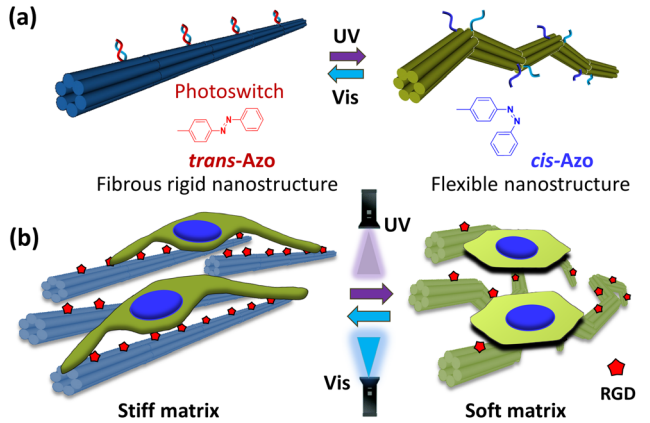

Fig. 1 Photoresponsive 3D tunable nanotubes as a tunable stiffness ECM for controlling cell morphology. (a) Schematic representation of DNA nanotubes containing azobenzene photoswitches and the predicted conformation change when the DNA nanotubes are subjected to UV/VIS irradiation. (i) Upon VIS light irradiation, a fibrous DNA nanotube is predicted when azobenzene moieties are in the *trans* state, (ii) upon UV light irradiation the azobenzene takes up *cis* conformation and destabilizes the duplex resulting in flexible DNA nanotubes (b) illustration of cell morphology change using photocontrolled DNA nanotubes. DNA nanotubes when used as a substrate for cell culture are expected to be perceived by the cells as a stiffness tunable matrix; a stiff nanoscaffold with fibrous DNA nanotubes and a soft nanoscaffold with flexible DNA nanotubes are reversibly formed using UV/VIS irradiation.

Fig. 2a, the nanotube unit (21 nm) was designed with a split in the middle (indicated by Open) (Fig. S1†). When the switching strands on the top hybridize, the split nanotube unit connects. The nanotube unit was also designed to multiply and assemble into a fibrous nanostructure. The two nanotube units are kept physically together by the strands spanning the bundle. By using this design, if the switching strands do not form a duplex, the DNA nanotube should fail to form the fibrous nanostructure, resulting in a flexible and undefined nanostructure. It is important to note that the perfect alignment of all helices of the bundle would make the bundle rigid and this is possible only if the two switching strands hybridize one another. In the case when the strands do not hybridize, several nicks present along the same axis makes the structure flexible. Initially, we designed some control DNA nanotubes to study our hypothesis. The control nanotubes were labelled as follows (Fig. 2b): (i) nanotube, (ii) nanotube with complementary switching strands 1 and 2, and (iii) nanotube with switching strand 1 only. These control tubes were annealed and observed under a AFM (Fig. 2b). It was observed that the usual nanotube formed fibrous nanostructures (up to 200 nm) with two-layer height (Fig. 2b (i) and Fig. S2†). Furthermore, in accordance with our hypothesis, DNA nanotubes held together by a DNA duplex *i.e.* nanotubes with switching strands 1/2 formed fibrous nanostructures (Fig. 2b (ii)), whereas nanotubes with only switching strand 1 formed flexible nanostructures when observed under a AFM (Fig. 2b (iii)).

We next extended our idea to an azobenzene photoswitch-containing DNA nanotubes (Azo-nanotube) (Fig. 3). Here we hypothesized that when the azobenzene moieties are in the *trans*-form, a duplex can be formed between the azobenzene containing strand (3-Azo) and switching strand 1, and thus the fibrous rigid nanostructure of the DNA nanotubes was expected to be formed. When the azobenzene strand (3-Azo) is irradiated with UV light, the azobenzene moieties take up the *cis*-form to induce the duplex dissociation, thus leading to the formation of flexible nanostructures.

Studying the change in the conformation and reversibility of photocontrolled mechanical DNA nanotubes

The nanostructure changes of the assembled Azo-nanotubes were studied using AFM. The nanotubes were annealed from 80 °C to 60 °C at a rate of 0.5 °C min^{-1} and then at 60 °C to 15 °C at a rate of 0.1 °C min^{-1} in a buffer containing 20 mM Tris-HCl (pH 7.6) and 25 mM $MgCl_2$. We used an LED light source [(365 nm (UV) and 450 nm (VIS)] equipped with an optical fiber for the photoirradiation experiment. The annealed sample was divided into 3 parts—(i) sample 1—taken immediately after annealing (whereby the azobenzene moieties are in the *trans* conformation), (ii) sample 2—annealed sample with UV irradiation at 37 °C for 10 min (365 nm), and (iii) sample 3—annealed sample with UV irradiation at 37 °C for 10 min and subsequent VIS irradiation at 37 °C for 10 min. All the samples were then observed using AFM. As shown in the AFM images, there was a clear change in the conformations of sample 1 and sample 2, and sample 3 showed a reversion in the structure of the Azo-nanotubes to the fibrous structure. The AFM images showed that there was a conformation change in the Azo-nanotubes from fibrous to flexible and then back to fibrous (Fig. 3 and S3†).

Thereafter, we manually counted the number of nanotubes that changed their conformation and plotted the efficiency of conversion and reversal (Fig. 3b). It was observed that the conversion efficiency of fibrous nanotubes to flexible nanotubes was around 91.3% and the reformation of fibrous nanotubes yielded an efficiency of around 46% (Fig. 3b). The results indicate that the fibrous and flexible morphologies of the nanostructures could be controlled by UV/VIS irradiation.

Next, we also measured the persistence length of the Azo-nanotubes in the initial, UV-irradiated and UV-VIS irradiated states. Image J was used to measure the length and persistence lengths were calculated from the AFM images based on a previously reported method.[13–15] The persistence lengths of the Azo-nanotubes in the initial state were calculated to be 17.9 ± 3.7 nm, in the UV irradiated state the persistence lengths were reduced to 4.1 ± 2.2 nm and in the UV-VIS state the persistence lengths were estimated to be 15.0 ± 4.1 nm. Persistence length, *i.e.* the mechanical property that quantifies the bending stiffness of a polymer[16] was observed and the structures changed drastically from the fibrous to the flexible state and from the flexible state back to the fibrous one. Thus, the Azo-nanotubes changed their structural conformation among the three states.

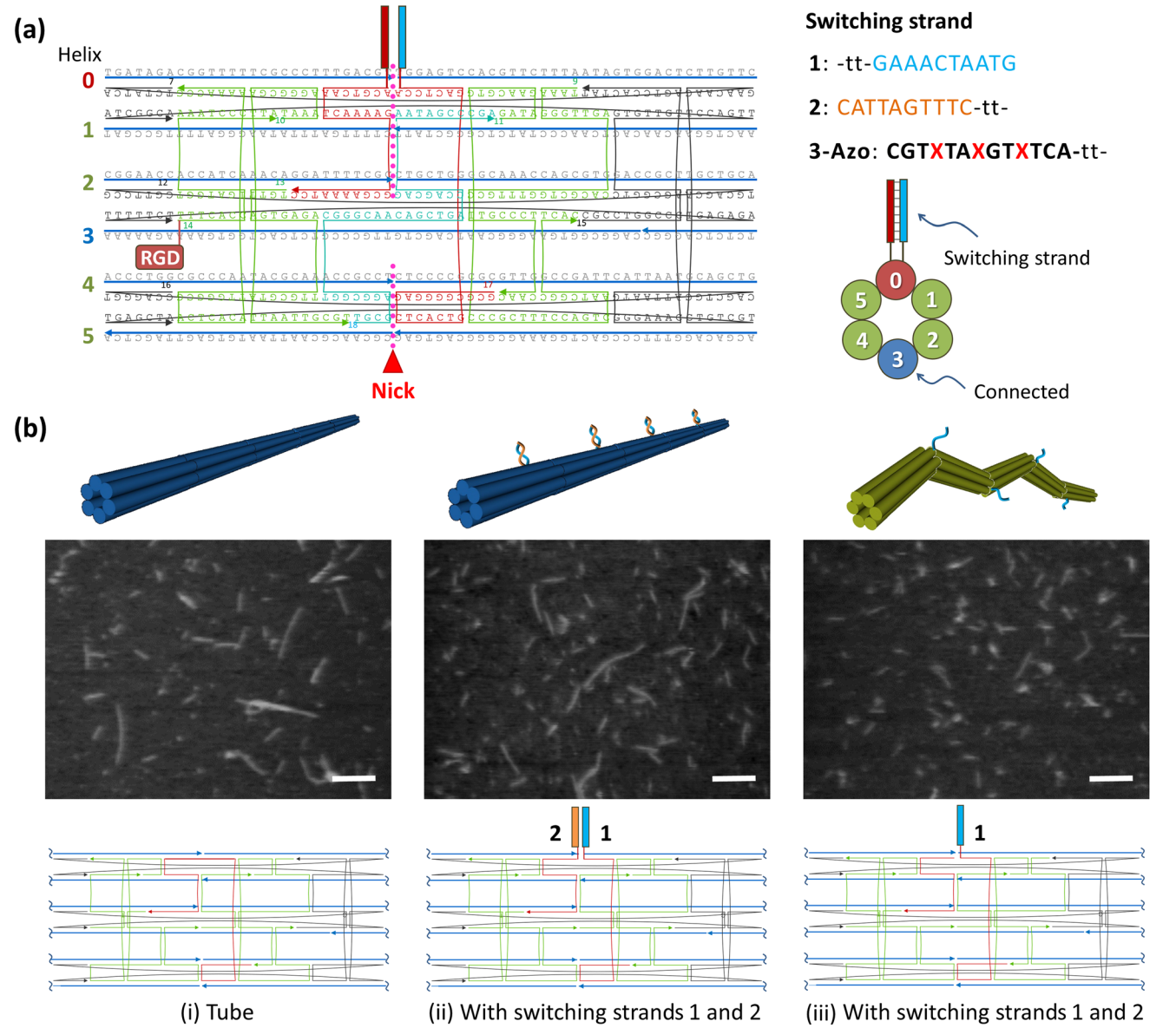

Fig. 2 Design and control of the structure of DNA nanotubes. (a) Design of the six-helix bundled DNA nanotube containing switching strands and RGD ligand. Switching strands are indicated as long rectangles. The DNA nanotube was designed using the caDNAno software. Only Helix 3 is connected, while the other helices are disconnected at the center (indicated by Nick) to open the tube. Switching strands on Helix 0 control the open/close of the tube. (b) AFM images of the DNA nanotubes. (i) Unmodified DNA nanotube. Fibrous nanostructures were observed. (ii) DNA nanotube assembled with switching strand 1/2. Fibrous nanostructures were observed. (iii) DNA nanotube assembled with switching strand 1 only. Flexible nanostructures were observed. Scale bars: 100 nm.

Photocontrolled mechanical DNA nanotubes with multivalent cell binding peptides

To facilitate cell binding and spreading onto the formulated DNA nanotubes, they were conjugated to RGD (cyclic Arg–Gly–Asp) peptide. RGD is a peptide sequence which is a part of the cell binding domain of fibronectin and has been previously reported to effectively bind to the cells through integrin receptors.[17] The peptide was conjugated to the DNA using a heterobifunctional linker sulfo-SMCC and then purified using HPLC (Fig. S4†). We also observed the nanostructure changes of RGD-conjugated Azo-nanotubes upon photoirradiation (Fig. S5†). The structural changes showed a similar tendency as compared to those with Azo-nanotubes, indicating that the RGD modification did not disturb the formation and photo-induced nanostructure changes.

Next, we investigated the presence of RGD peptide on the DNA nanostructure (incorporated position indicated by RGD in Fig. 2a). HeLa cells were seeded on fibrous DNA nanotube-coated surfaces. The negative control for this experiment was surface-coated with fibrous DNA nanotubes without any RGD peptides incorporated. As a positive control, HeLa cells plated

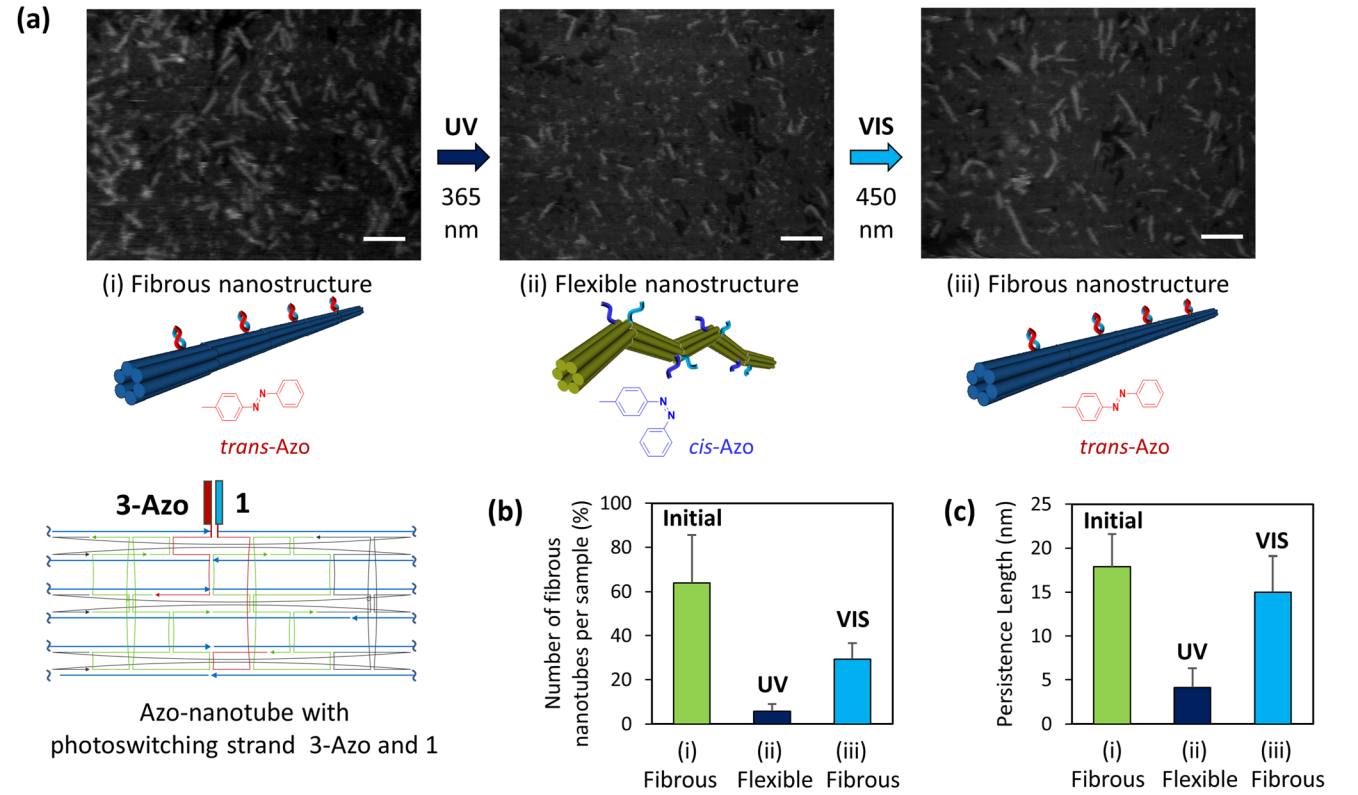

Fig. 3 DNA nanotube with azobenzene-photoswitches (Azo-nanotube). (a) AFM images of the Azo-nanotubes with the photoswitching strand 3-Azo and its complementary strand 1. (i) Fibrous nanotubes after annealing (initial state, *trans*-form). (ii) Flexible nanostructure after UV irradiation (*cis*-form). (iii) Reformation of fibrous tubes after VIS irradiation (*trans*-form). Scale bars: 100 nm. (b) Efficiency of the conversion of fibrous Azo-nanotubes to flexible nanotubes upon UV irradiation and re-conversion to fibrous Azo-nanotubes upon VIS irradiation was calculated and plotted. Error bars represent SD calculated based on three different samples. (c) Persistence length of the assembled Azo-nanotubes upon UV and VIS irradiation was calculated and plotted. Error bars represent SD calculated based on three different samples.

on a cell culture dish were chosen. The HeLa cells were seeded and allowed to attach and spread onto the surfaces. After 12 h of the experiment, the cells were fixed and stained with F-actin and a nucleus stain and visualized under a confocal microscope. As seen in ESI Fig. S6,† the cells readily adhered on all three substrates but the cell spreading was evidently more on DNA nanotubes containing RGD-coated surfaces when compared with DNA nanotubes without RGD-coated surfaces. From this result, we could confirm that the RGD–nanotube was successfully incorporated into the DNA nanotubes and the presence of RGD on the DNA nanotubes allowed the cells to spread and adhere well.

Reversible control of HeLa cell morphology using photoresponsive mechanical DNA nanotubes

We next investigated the effect of conformation changes between fibrous and flexible nanotubes on HeLa cells (Fig. 4a). The nanotubes were annealed from 80 °C to 60 °C at a rate of 0.5 °C min^{-1} and then at 60 °C to 15 °C at a rate of 0.1 °C min^{-1}. The prepared nanotubes were directly coated onto APTES-coated coverslips at a high concentration such that they can collectively be perceived as a matrix by the cells. After several hours of coating, the HeLa cells were seeded onto the fibrous rigid matrix, followed by UV light (365 nm, 10 min at 37 °C) irradiation to cause a conformation change of the fibrous rigid matrix to a flexible soft matrix and then VIS light irradiation (450 nm, 10 min at 37 °C) to cause re-formation of the fibrous rigid matrix. It was observed that the HeLa cells had a small cell body and long filopodia protrusions on the fibrous rigid matrix (Fig. 4a(i)), whereas on the flexible matrix the cells had a larger cell body and small filopodia protrusions (Fig. 4a(ii)). When the fibrous rigid matrix was reformed, the cells also responded and returned to having small cell bodies and long filopodia protrusions (Fig. 4a(iii)). This was a very interesting result as the dynamic hair-like cell protrusions called filopodia, also known as the sensory organelles of the cell, are the first component of the cell to establish contact with the extracellular matrix cues. Changes in their length and number confirm that the cell experiences a change in the cues from the ECM. These 3D DNA nanotube formed matrix is the first example of self-assembled nanostructures to provide 3D nanoscopic changes to the cells.

In addition, the changes in the morphology were accessed and the area occupied by the cells was calculated. Furthermore, the average length of filopodia was calculated and compared for all three states (Fig. 4b and c, and S7†).

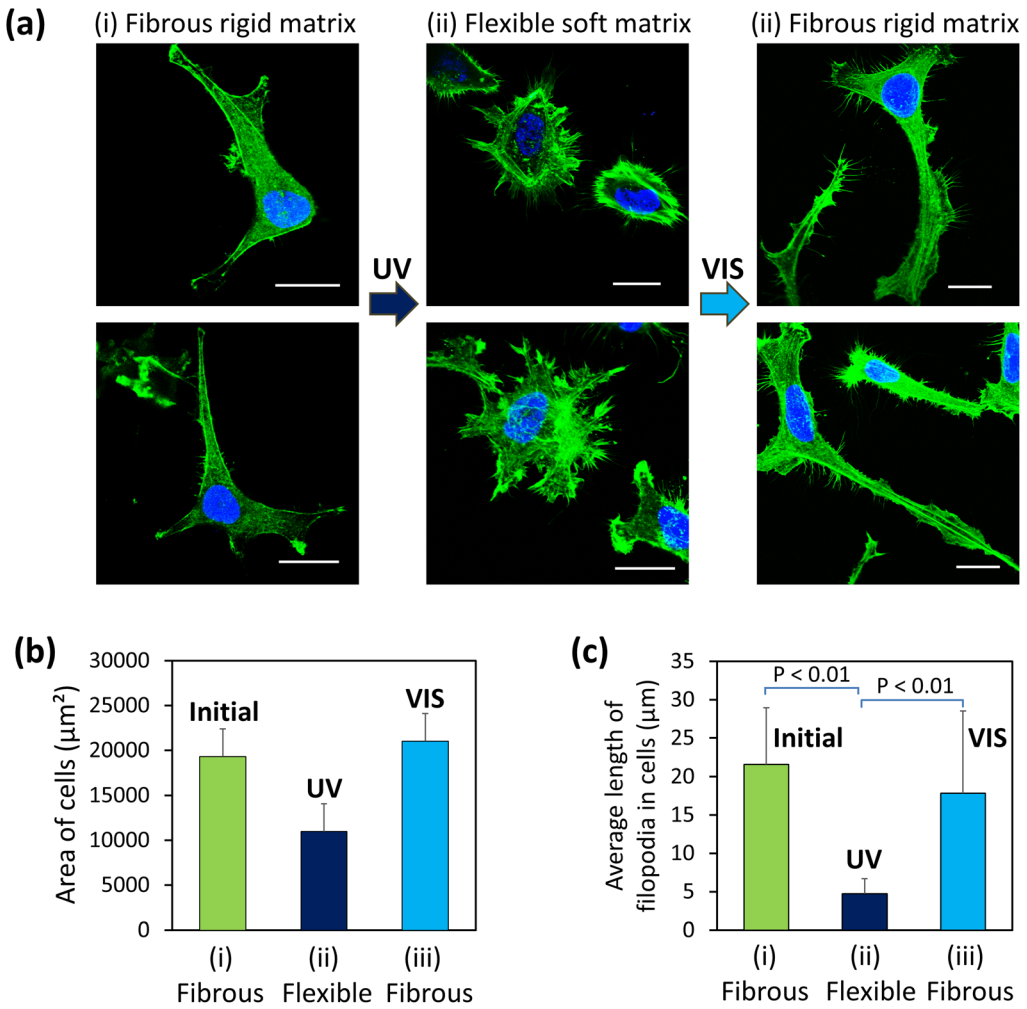

Fig. 4 Photoresponsive mechanical switching of RGD-conjugated Azo-nanotubes to control cellular morphology. (a) Representative images of HeLa cells cultured on three different states of DNA nanotube matrix (fibrous, flexible, and fibrous). Cell nuclei are stained in blue (DAPI staining) and F-actin is stained in green (FITC-labelled phalloidin staining). Scale bar: 20 μm. (b) Area under the cells cultured on the three substrates is calculated using image J. 50 cells were analysed for each sample. Error bars represent SD calculated based on three independent experiments. (c) Average length of filopodia was calculated and compared. 50 cells were analysed for each sample. Error bars represent SD calculated based on three independent experiments. *P* values of the samples were calculated for ensuring statistical significance and *P* value was observed to be less than 0.01 in each case.

Thus, it was observed that a 3D matrix with equidistant RGD peptides could be reversibly tuned into a fibrous rigid matrix and a flexible matrix for the cells. The results indicate that the matrix fibrosity and flexibility determined the cell morphology, spreading and filopodia protrusions. Dynamic filopodia changes could be observed at different states of the matrix.

Next, we set out to confirm whether these changes are caused only because of the changes in the conformations of the DNA nanotube and not because of UV light or any other element in the experiment set up. Thus, two control experiments were established. To start with, we assembled control DNA nanotubes (Fig. 2b (i)) containing the RGD moiety. These control nanotubes do not contain any azobenzene moieties, and thus, they should not undergo a conformation change upon UV or VIS irradiation. Next, HeLa cells were seeded onto them and allowed to attach and spread. UV light (365 nm, 10 min at 37 °C) was irradiated and the cells were allowed to spread. We then investigated the morphology of HeLa cells under initial and UV irradiation conditions (Fig. S8†). More than 50 cells were observed in each case and it was observed that even after UV irradiation, the HeLa cell morphology remained unchanged in the control DNA nanotubes with RGD. We also carried out a filopodia length analysis of the control samples (Fig. S6b†) and observed that the cells expressed similar size ranges of filopodia on the unmodified nanotubes. Furthermore, we examined the morphology of HeLa cells on pre-UV irradiated Azo-nanotubes (UV irradiation in solution). On the pre-UV irradiated flexible matrix (*i.e.*, flexible matrix), as expected the HeLa cells exhibited a round spherical shaped morphology (Fig. S9†) and upon calculation and comparison of the filopodia length with the control a significant difference was observed (Fig. S7c†). Thus, these control experiments con-

firmed that the cells were undergoing a morphological change only in response to the change in the conformation of the photoswitch-containing DNA nanotubes upon irradiation.

Conclusions

We have demonstrated that we can reversibly tune the stiffness of the matrix by changing the conformation of the photoresponsive mechanical DNA nanotubes using irradiation *i.e.* UV (365 nm) and VIS (450 nm), this conversion from a flexible soft matrix to a fibrous rigid matrix labelled with RGD peptide causes an overall change in the nanoscopic stiffness. These changes can be sensed by HeLa cells and they respond by changing the extent of spreading, morphology and size of filopodia-like extrusions. This dynamic and photocontrolled reversible DNA nanotube like matrix is a very useful tool as significantly less is known about the effects of matrix stiffening on cells in a 3D environment and can also be used for understanding the initial stages of the pathophysiology of many diseases and developmental processes. Such a dynamic 3D tunable matrix is crucial for expanding our knowledge about various cell–matrix phenomena and understanding the language of the ECM better.

Experimental

Materials

All the unmodified oligonucleotides were purchased from Eurofins Genomics (Tokyo, Japan). Azobenzene-containing DNA (3-Azo) was purchased from Japan Bio Services (Saitama, Japan). Cyclo-RGD [Cyclo(-RGDfK)] was purchased from ChemScene (Monmouth Junction, NJ, USA). SMCC (sulfosuccinimidyl-4-(*N*-maleimidomethyl)cyclohexane-1-carboxylate) was purchased from ThermoFisher Scientific (Waltham, MA, USA) and TCEP (trichloroethyl phosphate) was purchased from TCI (Tokyo, Japan). FITC-labelled phalloidin was purchased from Sigma-Aldrich (St Louis, MO, USA). An FV1200 laser scanning microscope (Olympus) was used for fluorescence imaging. A NanoDrop 2000c UV-Vis spectrophotometer was used for measuring the nucleic acid concentration.

Nanotube assembly

The nanotubes were designed using caDNAno and the sequences are listed in Tables S1 and S2†. The nanotubes were assembled in a 20 μL solution containing 5 μM of tube strands 1–6, 5 μM of tube strand 7, tube strands 9–16, and tube strand 18 and 5 μM of tube strand 8-Azo and tube strand 17 with switching strand 2 by annealing at 80 °C to 60 °C at a rate of 0.5 °C min^{-1} and then at 60 °C to 15 °C at a rate of 0.1 °C min^{-1} in a buffer containing 20 mM Tris HCl (pH 7.6) and 25 mM $MgCl_2$.

Photoirradiation to the nanotubes

For studying the conformation change, UV irradiation was carried out in a microtube at 37 °C for 10 min using a LED light source (CL-1501, Asahi Spectra). The LED used for UV irradiation was of the wavelength 365 nm (CL-H1-365-9-1, Asahi Spectra). The LED used for VIS irradiation was of the wavelength 450 nm (CL-H1-450-9-1, Asahi Spectra). The temperature during the irradiation was controlled using a temperature-controlled dry bath.

RGD conjugation to tube strand

Cyclo-RGD conjugation to tube strand 14 was performed using a previously described method.[17] The product was purified by HPLC and analysed by denatured PAGE (Fig. S3†).

AFM imaging and analysis

The AFM images were obtained using Dimension FastScan (Bruker AXS, Madison, WI) with a silicon nitride cantilever (Olympus BLAC10EGS). The samples were diluted using an observation buffer containing 20 mM Tris (pH 7.6), 25 mM $MgCl_2$, and 1 mM EDTA. The sample solution (10 μL) was adsorbed onto a mica plate for 5 min at rt and then washed three times with the same observation buffer. Scanning was performed in the same buffer solution in the tapping mode.

For calculating the persistence length, the formula reported previously was used. Nanotubes in the AFM images were manually counted and their lengths were calculated using the Image J software. The persistence length calculations were done for at least 50 nanotubes in each case.

Preparation and coating of glass slides

Glass slides used for the cell experiments were cleaned thoroughly using sonication in water, ethanol and water each for a duration of 10 min. Subsequently, the glass slides were etched by immersing them in a piranha solution, following which they were washed with water, ethanol and acetone. After the wash, they were coated with 1% APTES (in acetone) for 3 min and then washed 3 times in acetone. They were further dried in an oven at 120 °C for 2–3 h and then stored in a sterile environment for future use.

Cell culture

HeLa cells (JCRB Cell Bank Japan) were cultured and maintained in Dulbecco's Modified Eagle's Medium (ThermoFisher Scientific) supplemented with 10% fetal bovine serum (Sigma) and 1% penicillin/streptomycin. Incubation of the cells was done at 37 °C under a 5% CO_2 atmosphere with 95% humidity. A serum-free media supplemented with 1% insulin–transferrin–selenium (ThermoFisher Scientific) was used as we suspect that the use of fetal bovine serum might allow non-specific cell adhesions which might interfere with our results.

For the experiment, the cells were seeded on 4 substrates (sample 1 on a cell culture dish and sample 2, sample 3, and sample 4 on rigid DNA nanotube-RGD coated glass). The cells were seeded on all the substrates and allowed to adhere and spread for

3 h. Then, sample 2 and sample 3 were irradiated with UV light (365 nm) for 10 min while incubating the cells at 37 °C. Next, the cells were allowed to spread for 3 h and sample 3 was irradiated with VIS light at 450 nm for 10 min, while incubating the cells at 37 °C. After culturing the cells for another 3 h, the medium was aspirated from the wells and the cells were fixed using 4% paraformaldehyde. After fixing, the cells were washed with PBS three times and phase contrast images of each sample were taken.

UV-VIS exposure to cells

The UV and VIS irradiation were performed through a LED light source (CL-1501, Asahi Spectra). The LED used for UV irradiation was of the wavelength 365 nm (CL-H1-365-9-1, Asahi Spectra) and the light intensity used for the cell experiments was calculated as 16.416 mW cm^{-2} keeping into account the working distance and plate dimensions. The LED used for VIS irradiation was of the wavelength 450 nm (CL-H1-450-9-1, Asahi Spectra) and the light intensity used for the cell experiments was calculated as 14.22 mW cm^{-2} keeping into account the working distance and plate dimensions. It should be noted that the reported intensity has been calculated by keeping into account the 8–10% decrease when passed through polystyrene. During the entire time of irradiation, the cells were maintained at 37 °C.

Conflicts of interest

There are no conflicts to declare.

Acknowledgements

This work was supported by a Grant-in-Aid for Scientific Research (JSPS KAKENHI Fund 16H06356, 18KK0139, and 21H02057) to ME. Financial support from the Uehara Memorial Foundation and Heiwa Nakajima Foundation to ME was acknowledged.

References

1 S. W. Moore, R. E. Keller and M. A. R. Koehl, *Development*, 1995, **121**, 3131–3140.
2 M. Xue and C. J. Jackson, *Adv. Wound Care*, 2015, **4**, 119–136.
3 P. C. Georges, J. J. Hui, Z. Gombos, M. E. McCormick, A. Y. Wang, M. Uemura, R. Mick, P. A. Janmey, E. E. Furth and R. G. Wells, *Am. J. Physiol.: Gastrointest. Liver Physiol.*, 2007, **293**, 1147–1154.
4 J. Virga, L. Szivos, T. Hortobágyi, M. K. Chalsaraei, G. Zahuczky, L. Steiner, J. Tóth, J. Reményi-Puskár, L. Bognár and A. Klekner, *Oncol. Lett.*, 2019, **17**, 797–806.
5 K. R. Levental, H. Yu, L. Kass, J. N. Lakins, M. Egeblad, J. T. Erler, S. F. T. Fong, K. Csiszar, A. Giaccia, W. Weninger, M. Yamauchi, D. L. Gasser and V. M. Weaver, *Cell*, 2009, **139**, 891–906.
6 M. J. Paszek, N. Zahir, K. R. Johnson, J. N. Lakins, G. I. Rozenberg, A. Gefen, C. A. Reinhart-King, S. S. Margulies, M. Dembo, D. Boettiger, D. A. Hammer and V. M. Weaver, *Cancer Cell*, 2005, **8**, 241–254.
7 R. S. Stowers, S. C. Allen, L. J. Suggs and K. S. Anseth, *Proc. Natl. Acad. Sci. U. S. A.*, 2015, **112**, 1953–1958.
8 J. A. Burdick and W. L. Murphy, *Nat. Commun.*, 2012, **3**, 1269.
9 S. Sethi, K. Hidaka, H. Sugiyama and M. Endo, *Angew. Chem., Int. Ed.*, 2021, **60**, 20342–20349.
10 K. Zhang, R. Deng, Y. Sun, L. Zhang and J. Li, *Chem. Sci.*, 2017, **8**, 7098–7105.
11 D. Karna, M. Stilgenbauer, S. Jonchhe, K. Ankai, I. Kawamata, Y. Cui, Y. R. Zheng, Y. Suzuki and H. Mao, *Bioconjugate Chem.*, 2021, **32**, 311–317.
12 X. Liang, T. Mochizuki and H. Asanuma, *Small*, 2009, **5**, 1761–1768.
13 S. Mantelli, P. Muller, S. Harlepp and M. Maaloum, *Soft Matter*, 2011, **7**, 3412–3416.
14 D. Schiffels, T. Liedl and D. K. Fygenson, *ACS Nano*, 2013, **7**, 6700–6710.
15 P. W. K. Rothemund, A. Ekani-Nkodo, N. Papadakis, A. Kumar, D. K. Fygenson and E. Winfree, *J. Am. Chem. Soc.*, 2004, **126**, 16344–16352.
16 D. Karna, W. Pan, S. Pandey, Y. Suzuki and H. Mao, *Nanoscale*, 2021, **13**, 8425–8430.
17 M. D. Pierschbacher and E. Ruoslahti, *Nature*, 1984, **309**, 30–33.